DOI: https://doi.org/10.68732/988dbbd829f5e3e6

ISBN: 978-9989-2053-7-8

Predicting Fluid and Mechanical Response in 3D Discrete Fractures Using Graph Neural Network

Botong Du
Department of Geotechnical Engineering, College of Civil Engineering, Tongji University, China
dubotong@tongji.edu.cn
0009-0005-9227-7502

Zhao Feng
Department of Geotechnical Engineering, College of Civil Engineering, Tongji University, China

Fengshou Zhang
Department of Geotechnical Engineering, College of Civil Engineering, Tongji University, China

Bicheng Yan
Physical Science and Engineering Division, King Abdullah University of Science and Technology (KAUST), Saudi Arabia

Abstract

Accurate prediction of fluid flow and mechanical deformation in fractured rock formation is critical for deep subsurface projects. Although high-fidelity numerical simulations can resolve these coupled processes, their computational cost limits rapid screening and optimization of injection strategies. This study presents a graph neural network (GNN) based surrogate for predicting the hydro-mechanical response in 3D discrete fracture networks (DFNs). The DFN is represented as a fracture-level graph, in which fractures are modelled as nodes with features encoding fracture geometry and spatial context, and fracture intersections are represented as edges with features encoding network connectivity and topology. The training data are generated using a distinct element method simulator 3DEC, which solves coupled hydro-mechanical processes during hydraulic fracturing. Separate graph convolutional networks (GCNs) are trained to predict the node-wise average fracture aperture and pore pressure under different injection conditions. Results show that the surrogate achieves high predictive accuracy for both fracture aperture and pore pressure, with test R^2 values of 0.9937 and 0.9894, respectively. For aperture prediction, the mean absolute error (MAE) is 0.01 mm. The model captures the response of both the primary hydraulic fracture and natural fractures.The trained model delivers a prediction for a single scenario in approximately 6.43ms on a CPU, compared to the 11.5 h required by the simulator. The proposed workflow enables rapid estimation of the extent of activated fractures and permeability changes under varying operating conditions, providing a practical basis for injection parameter screening, optimization, and uncertainty analysis in fractured reservoirs.

Keywords

Graph neural network, Discrete fracture network, Surrogate model, Hydraulic fracturing, Reservoir stimulation.

1 Introduction

Hydraulic fracturing involves injecting high-pressure fluid into rock formations to create artificial fractures, stimulating low-permeability reservoirs to support subsequent production (Detournay 2016). In fractured reservoirs such as shale and granite, the stimulation objective is not only to form a primary hydraulic fracture, but also to activate pre-existing discontinuities to a highly connected fracture network (McClure and Horne 2014). Therefore, understanding fracture deformation behavior under different injection conditions is essential for predicting the resulting fracture network morphology and connectivity (Riahi et al. 2019).

Numerical simulation offers a controlled and physically interpretable approach for investigating hydraulic fracturing, enabling explicit description of fracture behavior under multi-physics coupling (Zhang et al. 2020). However, high-fidelity models typically require fine discretization and iterative solutions. The computational cost increases rapidly with fracture scale and complexity, making them infeasible for rapid engineering prediction and optimization (Lei et al.2017).

Surrogate models have been widely adopted to replace or accelerate high-fidelity simulations (Karniadakis et al. 2021). Most established workflows employing convolutional neural networks (CNNs) have shown strong capability in prediction, inversion, and optimization tasks (Tang et al. 2020). However, CNNs typically require both inputs and outputs to be represented as structured fields. For fractured reservoirs where connectivity is inherently non-Euclidean, CNNs can be inefficient (Bronstein et al. 2017). Graph neural networks (GNNs) offer a natural representation for such problems, and message-passing models have demonstrated accurate and efficient surrogate simulation on unstructured discretizations (Pfaff et al. 2021).

In this study, we develop a novel graph-based surrogate workflow for hydraulic stimulation in a three-dimensional fractured reservoir. The discrete fracture network (DFN) is converted into a fracture-level graph, and a graph convolutional network is trained to predict averaged aperture and pore pressure within each fracture under varying injection conditions. The surrogate model provides accurate estimates of the activated-fracture extent and permeability evolution in milliseconds, enabling efficient injection-parameter screening, optimization, and uncertainty analysis.

2 Graph dataand GNN model

2.1 Distinct element simulation model

Calculating the response of fractured reservoirs under hydraulic fracturing requires consideration of multiphysics evolution in discontinuous media. In this study, a three-dimensional distinct element code(3DEC) is adopted to simulate the hydro-mechanical behavior of the fractures in reservoirs (Itasca Consulting Group, Inc. 2020). This method has been validated in prior work for fully coupled hydro-mechanical problemsby comparison with analytical benchmarks (Dontsov and Zhang 2018).

Fig. 1 a) shows the dimensions of the numerical model, with a total size of 120 m × 120 m × 120 m, and a core region of 60 m × 60 m × 60 m. To represent natural fractures, we construct a 3D DFN. Fracture orientations and intensity are constrained by field drilling data, while fracture sizes are sampled from a power-law distribution. Simplification measures are applied to the DFN to ensure the mesh quality of the model (Du et al. 2025). Ultimately, three major groups of natural fractures are considered in the model, as illustrated in Fig. 1 b).There are 61 fractures in each sample. Primary hydraulic fracture (blue fracture) is approximated by a pre-defined vertical fracture planein the middle of the model, oriented parallel to the maximum horizontal principal stress (S_H), NE40°. The DFN and the primary hydraulic fracture plane are initially pre-bonded with their corresponding strength and subsequently undergo localized failure during fluid injection as stress conditions change.

As for the model properties, a Young's modulus of 43 GPa, Poisson's ratio of 0.21, and density of 2600 kg/m^{3}are used for the intact rock properties of granite. The injection point is set at the middle of the model at a depth of 3700 m.At the model center, the maximum horizontal principal stress, minimum horizontal principal stress, and vertical principal stress are 111 MPa, 92 MPa, and 92 MPa, respectively. The initial pore pressure is calculated from a hydrostatic gradient of 9.81 MPa/km, corresponding to 36.3 MPa at the injection depth. Fluid flow is solved within the connected fracture network and is coupled with fracture deformation through aperture changes during injection. This

setting allows the model to capture both pressure diffusion and mechanically induced fracture opening in the DFN. The modelis discretized into approximately 180,000 zones in total.

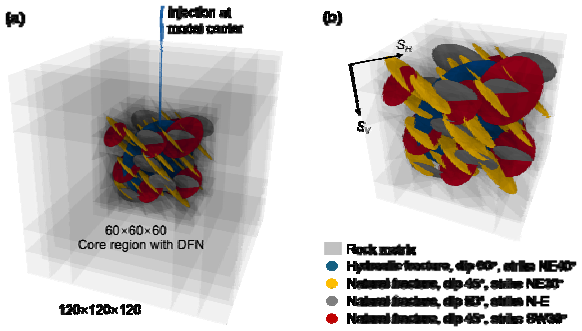


Fig. 1a) Whole model and b) Core region with discrete fracture network in the numerical model.

2.2 DFN-based graph dataset

To enable learning on irregular fracture geometries, each discrete fracture network is represented as an attributed graph at the fracture level, as illustrated in Fig. 2. Each fracture is mapped to one node located at its geometric centroid. Two nodes are connected if the corresponding fractures intersect in the DFN. Under this definition, each graph contains 61 nodes and 107 edges, which preserves the connectivity pattern of the fracture network while keeping the representation compact.

Node features encode fracture geometry and spatial context. Specifically, we use centroid coordinates and fracture descriptors, including size, dip, strike, and the distance to the injection well. These features provide the model with both local orientation information and global positioning within the reservoir. Edges carry a single spatial attribute, defined as the Euclidean distance between the centroids of two intersecting fractures. Each graph sample also includes three graph-level operating variables, including injection rate, fluid viscosity, and cumulative injected volume. The injection rate and viscosity are sampled using Latin hypercube sampling over 0.01–0.2 m³/s and 0.001–0.1 Pa·s, respectively. In total, 200 independent 3DEC simulations are performed. For each simulation, 15 states are extracted from the transient response at cumulative injected volumes of 2, 4, ..., and 30 m³, yielding 3000 graph samples.

The prediction targets are the average fracture aperture and the average pore pressure. We train two separate models to predict the two targets individually. These fracture averaged quantities are adopted because each node represents one fracture, and they are sufficient to characterize the overall activation extent and response pattern of the stimulated fracture network. The 3000 graph samples are randomly split into 2100, 450, and 450 graphs for training, validation, and testing.

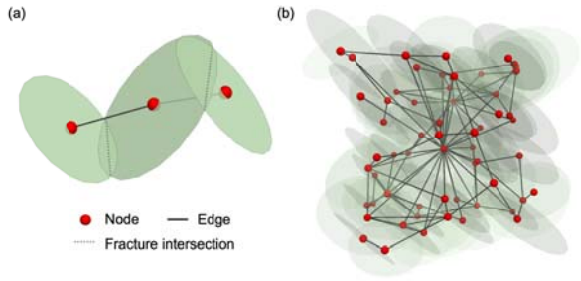


Fig. 2a) Graph mapping of an intersecting fracture pair, where nodes denote fracture centroids and edges denote intersections, and b) Graph representation of a full fracture network sample.

2.3 GNN model

We build a graph convolutional surrogate model $\mathbf{f}_\theta$ to predict fracture scale responses under prescribed injection conditions. The surrogate is trained on high-fidelity samples generated by the coupled distinct element simulator $\mathbf{f}_h$. Given a DFN graph $\mathbf{G}$ with node features $\mathbf{x}_i$ and edge attributes d_{ij}, the model outputs a node-wise scalar $\hat{y}_i$, which corresponds to either the average pore pressure or the average fracture aperture of fracture i. We train two separate networks for the two targets.

The schematic is shown in Fig. 3. It contains four graph convolution blocks with hidden sizes 256, 256, 128, and 64, followed by a linear layer that maps each node embedding to one output value. A GCN layer updates node embeddings as

$$\mathbf{h}_i^{(l+1)} = \sigma\left(\sum_{j\in\mathcal{N}(i)\cup\{i\}} \alpha_{ij}^{(l)}\mathbf{W}^{(l)}\mathbf{h}_j^{(l)}\right) \quad (1)$$

Where $\mathbf{h}_i^{(l)}$ The node embedding of node i at layer l, with $\mathbf{h}_i^{(0)} = \mathbf{x}_i$

$\mathbf{x}_i$ Initial node and global features

$\mathcal{N}(i)$ Neighbor set of node$i$

$\alpha_{ij}^{(l)}$ Normalized aggregation coefficient between nodes i and j at layer l

$\mathbf{W}^{(l)}$ Learnable weight matrix at layer l

$\sigma(\cdot)$ ReLU activation function

GraphNorm is applied after each convolution to normalize node embeddings within each graph in a mini batch, which reduces scale variation across DFN samples and stabilizes training. Dropout with a rate of 0.15 is applied after ReLU. The edge attribute is a single scalar distance d_{ij}, defined as the Euclidean distance between the centroids of two intersecting fractures. All node-level and graph-level input features are scaled to the range from 0 to 1 using min-max normalization. Model parameters θ are optimized by minimizing the mean squared error over all nodes in a mini-batch.We use the Adam optimizer with learning rate 1e−3 and weight decay 1e−4.

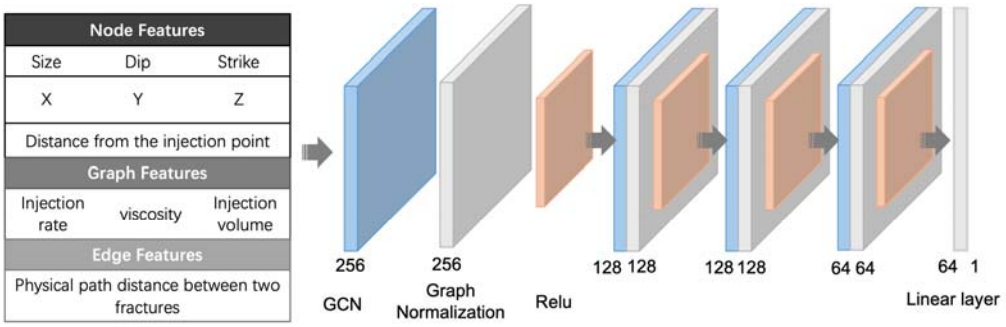


Fig. 3 Schematic of theforward graph convolutional network model.

3 Results and discussion

The surrogate model $\mathbf{f}_\theta$aims to predict the average aperture or pore pressure of each fracture surface. This enables rapid delineation of the activated fracture network under a given injection condition and supports subsequent parameter screening and optimization. Training of $\mathbf{f}_\theta$ is performed with a batch size of 128 for up to 150 epochs. Fig. 4 reports the learning curves and test performance for the aperture task. The model converges within a few tens of epochs and maintains a high validation accuracy. On the test set, it achieves R^2 = 0.9937 with RMSE = 0.0796 and MAE = 0.0443in the normalized space. After inverse scaling, the errors correspond to RMSE = 1.8 × 10^{-5} m and MAE = 0.01mm. The predicted and true values are closely distributed around the one-to-one trend, indicating accurate prediction of the surrogate. For pore pressure prediction, the model achieves a test R^2 = 0.9894 with RMSE = 0.1024 and MAE = 0.0563 in the normalized space. Since the test samples were not used during training, and the training and validation RMSE curves show similar convergence trends without clear separation, no evident overfitting is observed in the present dataset.

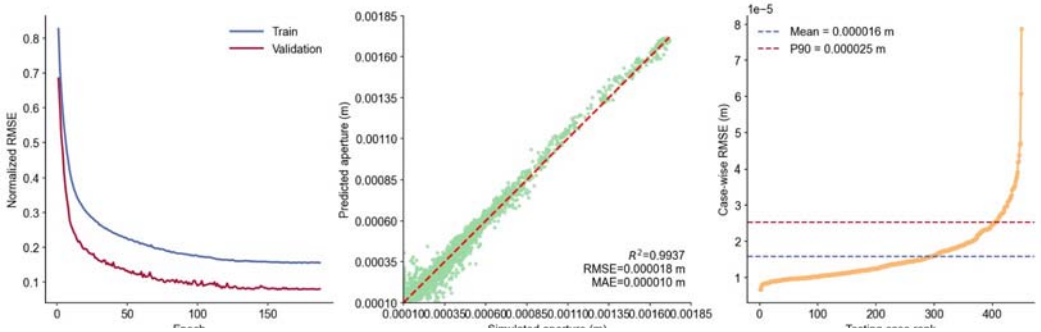


Fig. 4a) Training and validation RMSE curves; b) Predicted versus true aperture values on the test set; c) Ranked distribution of case-wise RMSE for all testing cases.

Using test sample 376, we compare the surrogate predictions $\mathbf{f}_\theta$ against the high fidelity simulator $\mathbf{f}_h$ to illustrate the node-wise aperture accuracy. This case corresponds to an injection rate of 0.0502m³/s, viscosity of 0.0052Pa·s, and injection volume of 28 m³. The error is defined as the absolute difference between predicted and simulated values, which directly reflects the magnitude of deviations relevant to engineering use. Fig. 5 visualizes the predicted and simulated aperture field, and the distribution of absolute errors. The surrogate model reproduces both the primary hydraulic fracture and the surrounding natural fractures with good agreement. The maximum absolute error is below 0.1 mm, which indicates that the surrogate preserves the overall amplitude of the aperture response while introducing only small local deviations.

This efficiency gain is substantial for practical workflows that require repeated evaluations under different injection conditions. For this case, the surrogate inference takes 6.43 ms on a CPU for one graph, while the corresponding fully coupled simulation requires about 11.5 h. This yields an approximate speedup of 6.4×10^6 for single case evaluation. As a result, the surrogate enables rapid prediction of the activated DFN extent under a given scenario and provides an efficient approximation of the aperture and permeability distribution for downstream screening and optimization.

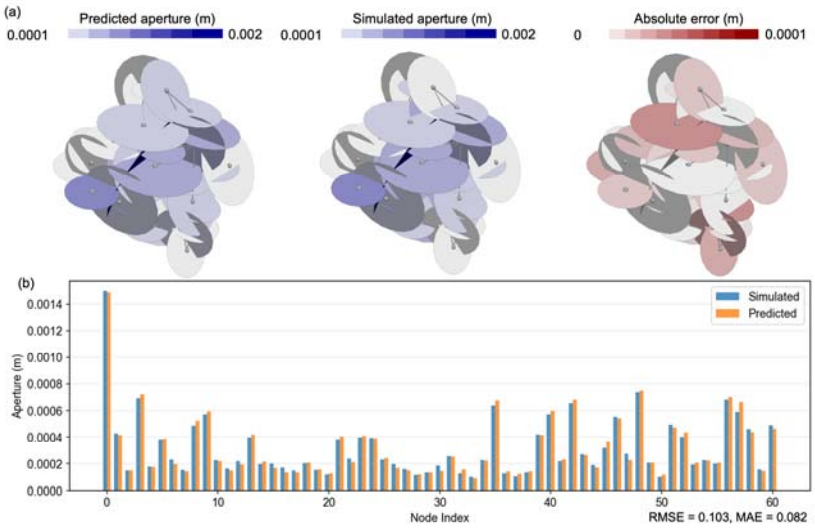


Fig. 5 Fracture average aperture for test sample 376 with injection rate 0.0502m³/s, viscosity 0.0052Pa·s, and injected volume 28 m³:a) Predicted aperture, simulated aperture, and absolute error mapped on DFN; b) Node-wise comparison of predicted and simulated aperture values.

It is worth noting that sample 376 is not among the best predicted cases, with its case-wise RMSE ranking 383rd out of 450 testing cases in Fig. 4c). We report it because it is more representative of practical operating conditions that are harder to predict. In cases with low injection rate and viscosity but large injected volume, more natural fractures are activated. Many of these fractures are near the activation boundary and occur less frequently across the dataset. The strong performance on this case suggests that the surrogate remains reliable under more complex activation patterns.

The training and testing results also reveal several limitations. Although the average test MAE is small, a few outlier cases still show noticeably larger errors, with MAE reaching about 0.3 in the normalized space. This behavior is primarily attributed to the limited coverage of the data manifold. Future work will also evaluate robust loss functions to further reduce the influence of outlier cases during training. Some fractures are activated only under a narrow set of injection conditions, which results in fewer informative samples for learning their response. In addition, since the current graphs are small, a basic GCN is sufficient for both efficiency and accuracy. For field-scale applications with substantially more fractures and more heterogeneous connectivity, richer edge features or more expressive message passing architectures may be required. Addressing these challenges will require larger and more diverse high-fidelity simulation datasets. However, generating such datasets also places higher demands on the numerical simulator in terms of computational cost and convergence robustness.

Also, the current learning target is the fracture averaged aperture or pore pressure. This formulation is sufficient for fast estimation of the activated fracture extent and fracture permeability changes. It does not yet provide a detailed spatial distribution of pressure and permeability in the stimulated reservoir. Ongoing work will extend both the simulation outputs and the learning formulation toward larger-

scale and higher-resolution predictions, with the goal of enabling more accurate assessments of reservoir stimulation outcomes under realistic engineering conditions.

4 Conclusion

This study presents a graph neural network surrogate for rapid prediction of fracture scale hydro-mechanical responses in 3D discrete fracture networks. High-fidelity datasets are generated using fully coupled distinct element simulations, and each DFN is mapped to a graph where nodes represent individual fractures and edges represent intersections. Conditioned on fracture geometry, spatial context, and injection parameters, the surrogate predicts node-wise average aperture and pore pressure with high accuracy. For the aperture task, the model achieves $R^2 = 0.9937$ on the test set, with RMSE $= 1.8 \times 10^{-5}$ m in physical units. Compared with the high-fidelity simulator that requires hours for a single run, the surrogate delivers predictions within milliseconds on a CPU, enabling efficient screening of injection scenarios and supporting future optimization workflows. Remaining errors are mainly associated with fractures that are rarely activated in the dataset and thus underrepresented during training. Future work will expand the simulation database to larger and more complex DFNs and extend the learning targets from fracture averaged quantities to higher resolution fields.

References

Bronstein MM, Bruna J, LeCun Y, Szlam A, Vandergheynst P (2017) Geometric deep learning: Going beyond Euclidean data. IEEE Signal Processing Magazine 34(4): 18–42. DOI:10.1109/MSP.2017.2693418.

Detournay E (2016) Mechanics of hydraulic fractures. Annual Review of Fluid Mechanics 48: 311–339. DOI:10.1146/annurev-fluid-010814-014736.

Dontsov EV, Zhang F (2018) Calibration of tensile strength to model fracture toughness with distinct element method. International Journal of Solids and Structures 144: 180–191. DOI:10.1016/j.ijsolstr.2018.05.001.

Du B, Zhang F, Zhang C (2025) Distinct element modeling of hydraulic fracture propagation with discrete fracture network at Gonghe enhanced geothermal system site, northwest China. Journal of Rock Mechanics and Geotechnical Engineering 17(6): 3435–3448. DOI:10.1016/j.jrmge.2024.04.028.

Itasca Consulting Group, Inc. (2020) 3DEC: Three-dimensional distinct element code, version 7.0. Itasca Consulting Group, Minneapolis, MN.

Karniadakis GE, Kevrekidis IG, Lu L, Perdikaris P, Wang S, Yang L (2021) Physics-informed machine learning. Nature Reviews Physics 3(6): 422–440. DOI:10.1038/s42254-021-00314-5.

Lei Q, Latham J-P, Tsang C-F (2017) The use of discrete fracture networks for modelling coupled geomechanical and hydrological behaviour of fractured rocks. Computers and Geotechnics 85: 151–176. DOI:10.1016/j.compgeo.2016.12.024.

McClure MW, Horne RN (2014) An investigation of stimulation mechanisms in Enhanced Geothermal Systems. International Journal of Rock Mechanics and Mining Sciences 72: 242–260. DOI:10.1016/j.ijrmms.2014.07.011.

Pfaff T, Fortunato M, Sanchez-Gonzalez A, Battaglia PW (2021) Learning mesh-based simulation with graph networks. International Conference on Learning Representations, Virtual Event, 3–7 May 2021. DOI:10.48550/arXiv.2010.03409.

Riahi A, Pettitt W, Damjanac B, Varun, Blanksma D (2019) Numerical modeling of discrete fractures in a field-scale FORGE EGS reservoir. Rock Mechanics and Rock Engineering 52(12): 5245–5258. DOI:10.1007/s00603-019-01894-6.

Tang M, Liu Y, Durlofsky LJ (2020) A deep-learning-based surrogate model for data assimilation in dynamic subsurface flow problems. Journal of Computational Physics 413: 109456. DOI:10.1016/j.jcp.2020.109456.

Zhang F, Yin Z, Chen Z, Maxwell S, Zhang L, Wu Y (2020) Fault reactivation and induced seismicity during multistage hydraulic fracturing: Microseismic analysis and geomechanical modeling. SPE Journal 25(2): 692–711. DOI:10.2118/199883-PA.